

## Abstract

Non-oxidative methane activation is carried out in a microwave plasma reactor for coupling to higher hydrocarbons. Fourier transform infrared spectroscopy (FTIR) was used to measure absolute concentrations of the major hydrocarbon species. Hydrogen concentration was also independently inferred from pressure based change in molar flow measurements. By closing both the carbon and hydrogen balance, from stoichiometry of the reactions, the amount of deposits was obtained as well. Additionally, core gas temperatures up to 2500 K were measured with Raman scattering when nitrogen acted as probing molecule in sample mixture discharges. At low gas temperatures, ethane and ethylene were significant products based on plasma chemistry, with ethane selectivities reaching up to 60 %. At higher gas temperatures, thermal effects become stronger shifting the selectivity towards acetylene and deposits, resembling more with equilibrium calculations. The energy efficiency of the methane conversion reached up to 15 % from which 10 % represented coupling efficiency to higher hydrocarbons. It is concluded that there is an interplay between plasma and thermal chemistry where plasma generates radicals and final distribution is set by thermodynamics.

# Non-oxidative methane coupling to C<sub>2</sub> hydrocarbons in a microwave plasma reactor

T. Minea<sup>1</sup>, D.C.M. van den Bekerom<sup>1</sup>, F.J.J. Peeters<sup>1</sup>, E. Zoethout<sup>1</sup>,  
M.F. Graswinckel<sup>1</sup>, M.C.M. van de Sanden<sup>1</sup>, A.H.G. Cents<sup>2</sup>, L.  
Lefferts<sup>3</sup>, and G.J. van Rooij<sup>1</sup>

<sup>1</sup>Non-equilibrium Fuel Conversion, DIFFER, Eindhoven, 5612 AJ,  
The Netherlands

<sup>2</sup>Sasol, Group Technology, 1 Klasie Havenga road, Sasolburg 1947,  
South Africa

<sup>3</sup>MESA+, Faculty of Science and Technology, University of Twente,  
Enschede, 7500AE, The Netherlands

## 1 Introduction

Methane remains an underutilized raw material for production of fuels and chemicals, with the main use being combustion for heating or power generation.[1] Olefins like ethylene, the most produced chemical in the world with over 150 million tons per annum,[2, 3] come from steam catalytic cracking of large hydrocarbons feedstock, obtained from crude oil distillation. It is a multi step process where separation is required and where combustion products are formed as well. Alternatively, methane is converted into syngas (CO+H<sub>2</sub>) that is further transformed into hydrocarbons over iron or cobalt catalyst via Fischer Tropsch (FT) synthesis.[4, 5, 6] Single step non-oxidative methane conversion to higher hydrocarbons has been a challenging topic of study being referred to as the search for the chemist's "Holy Grail".[7, 8, 9]

The indirect routes for methane utilization come from the fact that it is one of the most stable molecules, being very difficult to activate. Methane is highly symmetric, with the carbon and hydrogen atoms forming a tetrahedral structure. It is a nonpolar molecule (it has no permanent dipole in view of symmetry) where charge interaction and electron transfer processes are unlikely. A high ionization potential (12.61 eV)

limits electron transfer as well. Thermodynamically, it is easier to break all the C-H bonds, i.e. decomposing methane into carbon and hydrogen, than selectively breaking one C-H bond and do radical coupling reactions.[10, 11]

Routes to methane coupling can be separated in two main categories: oxidative and non-oxidative. In view of thermodynamics, most of the methane coupling efforts concern the oxidative process over various catalysts to achieve selectivity.  $O_2$  is used to shift the thermodynamic equilibrium, leading to higher conversion.[12, 13, 14, 15, 16] Additionally,  $CO_2$  can be used as an oxidant. In this way an active surface oxygen is supplied (needed for hydrogen abstraction from methane), without the generation of an additional gas phase oxygen resulting in even higher  $C_2$  yields.[17, 18, 19] Hydrocarbons, especially olefins, oxidize faster than methane leading back to  $CO_2$  formation. Hence, oxidative processes have an inherent conversion-selectivity problem: high  $CH_4$  conversions (i.e. feeding large amounts of oxidizing agent) are associated with poor product selectivity. The trade-off between conversion and selectivity has led to insufficient yields for industrial application of less than 30%. Low hydrocarbon yields have prevented the industrial up-scaling of the oxidative methane coupling process.[20, 7] Finally, the oxidative processes are very much energy intensive: either via pure oxygen (air separation is very energy intensive) or via separating excess nitrogen from the products (in case of using air).

Non-oxidative methane coupling does not have the disadvantages of oxygen and combustion products but the conversion is very low because of thermodynamic constraints. High temperatures are needed to activate the stable methane molecules. The single step process follows an endothermic reaction called pyrolysis. Depending on the process conditions, the reaction products are distributed among acetylene, hydrogen and solid carbon. Thermal activation is not selective and therefore most of the time done with a catalyst (heterogeneous phase) to convert methane to higher hydrocarbons or aromatics. The main problem is again carbon formation (coking) that leads to deactivation of the catalyst and selectivity loss.[11, 21]

Methane pyrolysis has been optimized at an industrial scale in the form of Huels process, where thermal plasma provides efficient heating up to the high temperatures needed.[22] In the original Huels reactor in the 1940s, an electric arc discharge was used for acetylene production from natural gas. Although appreciable conversion efficiencies can be achieved, this process has as main drawback that the energy efficiency is rather low. Values up to 48 % have been reported, corresponding to a minimum of 8 eV per molecule of acetylene formed.[23]

Alternative to thermal plasma are the more promising routes of nonequilibrium plasma, possibly enhanced in combination with catalysis. For example, an increased 64 % energy efficiency for methane conversion in microwave plasma reactors was reported in the 1990s at the Kurchatov Institute.[24] [25] This record value is attributed to a contribution from the non-equilibrium nature of the plasma that promotes vi-

brational excitation. Power is more efficiently deposited into vibrational degrees of freedom of the feedstock molecules than to their translational degrees of freedom. The result is an inequilibrium between the translational (i.e. gas) temperature and the vibrational temperature, hence the term "nonequilibrium plasma". In this medium alternative, more efficient paths to dissociation are open, e.g. due to a reduced activation barrier for methane.

In follow up series of methane microwave plasma conversion experiments, done in similar 2.45 GHz reactors and pressure ranges, energy efficiencies were below the thermodynamic limit of approximately 50 %. A maximum of 38 % efficiency was obtained at pressures of 100 to 120 mbar, but for a lower energy input of 1.2 eV per molecule of CH<sub>4</sub>.<sup>[26, 27, 28]</sup> With increasing input power and pressure, selectivity shifted from more saturated hydrocarbons to formation of acetylene and deposits. High ethane selectivities up to 77 % among C<sub>2</sub> products were reported in a similar reactor, but for pressures below 50 mbar.<sup>[29]</sup>

In this work a consistent data set on methane conversion in a continuous microwave reactor was obtained by closing up both carbon and hydrogen balances. A common shortcoming in microwave plasma hydrocarbon reforming work has been the incomplete analysis of the products because of the afferent complexity, as it was highlighted in a review chapter on the topic.<sup>[28]</sup> Discharges were investigated in a "mild" regime, i.e. at low specific energy input (SEI) and pressure, with the aim of maintaining low gas temperatures and deposit rates. The rationale here was to create conditions favorable for nonequilibrium driven record efficiencies. Quantitative analysis was obtained from FTIR measurements of the effluent. Pressure based measurements of the molar flow changes allowed to account for the non-isochore nature of the methane chemistry. In effect the full product distribution could be obtained and related to the discharge parameters. Moreover, in-situ gas temperatures were obtained from Raman scattering by adding nitrogen to act as a probing molecule in sample mixture discharges.

## 1.1 Plasma driven methane chemistry

Many reviews exist in literature on the topic of molecular plasma chemistry, one of which can be found in Chapter 2 of the *Nonthermal plasma chemistry and physics* book.<sup>[30]</sup> Here we want to highlight the potential to reach for high efficiencies offered by the nonequilibrium plasma. Additionally, we look at what are the sources and sinks for the main radicals that are present in methane discharges.

The electrons in the plasma are accelerated by the electric field of the standing microwave and decelerated through collisions with neutral molecules. The energy gained between collisions characterizes the type of interaction, as shown in Figure 1. In the low energy range, up to 10 eV, the main power loss mechanism is represented

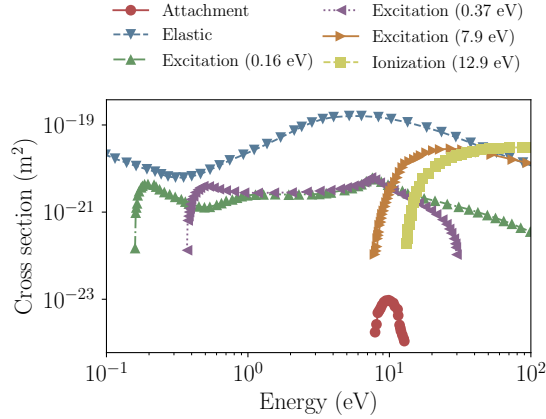
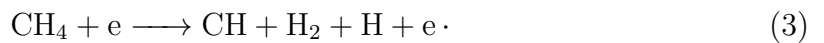


**Figure 1:** Electron impact cross sections in methane. Values in brackets represent threshold energies. Vibrational excitation has low energy thresholds of 0.16 and 0.37 eV, while electronic excitation and ionization have high energy thresholds of 7.9 and 12 eV.[31]

by vibrational excitation (elastic scattering does not count in the energy balance). In the high energy range, electronic excitation and ionization are dominant. Although ionization is needed to sustain the plasma, it should not become a significant part of the input energy (in view of the energy cost).

The high energy electronic excitations can also be dissociative, leading to formation of radicals. This happens within the electron energy distribution tail, from 9 eV onwards, where the following reactions are possible:



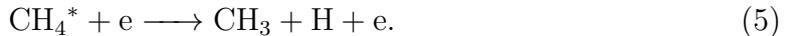
At even higher energies, direct decomposition can occur:



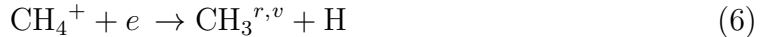
to directly produce carbon and hydrogen. Depending on the electron density and radical mean free path in the plasma, the radicals created in the above reactions can undergo further dehydrogenation leading to more carbon formation. Thus, both the electron temperature and density influence the outcome of the methane chemistry through the nature of created radicals.[32, 33]

The average C-H bond energy is around 4.5 eV. Direct electron impact dissociation is an inefficient process with more than half of the energy being lost into heat. A more efficient dissociation process would have an enhanced rate due to a lower activation

barrier, mediated by vibrational excitation[34]



Additional sources of methyl radicals are the dissociative recombination (DR) of methane ions [35]:



and hydrogen radical abstraction



A list of the ionization potentials for the main species in the plasma is given in Table 1. Methyl radicals have the lowest ionization potential among the possible radicals and hydrocarbon species present in the methane discharge. The DR process can represent also a loss channel for the radicals. Additionally, this process is responsible for making the electron temperature depending on input power in molecular plasmas. Minimizing the ionization from the molecular species by seeding alkali impurities (with low ionization potential) was suggested as a potential solution.[36]

Main sinks for H and CH<sub>3</sub> radicals are represented by three body reactions, as shown in Figure 2. Self-recombination to ethane and back reaction to methane are the dominant loss channels for methyl radicals. Hydrogen radicals are lost via methane dehydrogenation (methyl production), reaction 7, and self-recombination.

The dehydrogenation reaction can further apply to the formed products, leading to less saturated chains of hydrocarbons and soot:



Reactions 8-10 are identical to the last steps in the Kassel mechanism of methane pyrolysis. Methylene radicals are dominant in methane reduction within the Kassel mechanism as opposed to methyl radicals in plasma.[37, 25] Reactions 1-4 are responsible for the final product distribution through gas phase radical chain chemistry.

## 2 Experiment and Methodology

### 2.1 Experimental setup

The experimental setup consists of a microwave plasma reactor, a Fourier transform infrared (FTIR) spectrometer, a laser system and collection optics for the Raman scattering, as shown in 3. A brief description of the main components is given

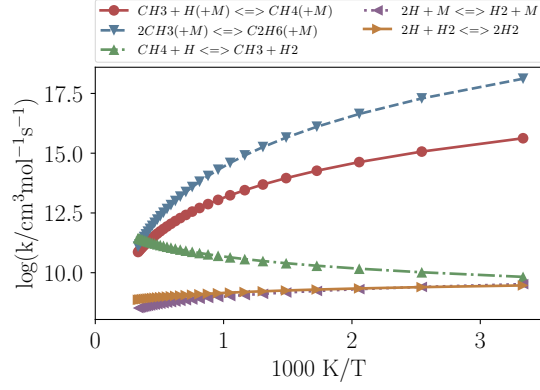


**Figure 2:** Selected radical loss rates from GRI-Mech 3.0 database. The pressure dependent reactions (+M) were taken at 0.1 atm in N<sub>2</sub>. [38]

**Table 1:** Ionization potential (eV) for radical and hydrocarbon species presented in the methane discharges.[39]

Species	IP (eV)
C	11.26
CH	10.63
CH <sub>2</sub>	10.40
CH <sub>3</sub>	9.84
CH <sub>4</sub>	12.61
C <sub>2</sub>	11.41
C <sub>2</sub> H <sub>2</sub>	11.40
C <sub>2</sub> H <sub>4</sub>	10.51
C <sub>2</sub> H <sub>6</sub>	10.52

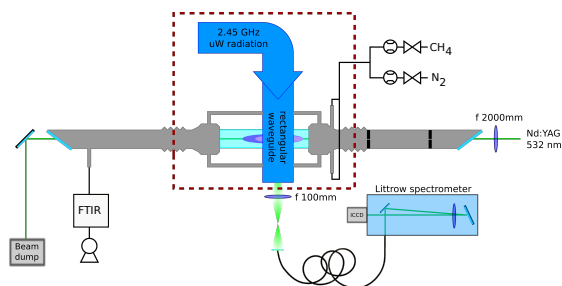


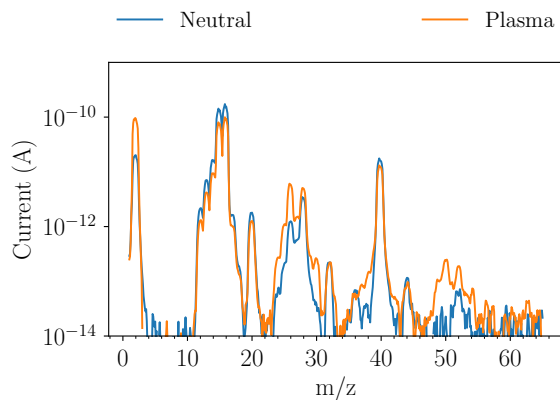
**Figure 3:** Schematic drawing of the microwave plasma plug flow reactor. Process gas is injected by means of two tangential injection nozzles connected to the upstream glass-to-metal connector on the quartz tube. The plasma is sustained in the tube by providing microwave radiation through a rectangular WR-340 waveguide. The FTIR sampling cell is 20.9 cm long and it is placed approximately 2 m downstream of the plasma together with the pressure gauge meter as well. Axial optical access for the Raman scattering is provided by two Brewster windows. A hole in the sliding short permits scattered light to be collected and finally coupled to the spectrometer via a linear fibre bundle.

here. A detailed description and operation of the microwave reactor, the FTIR sampling procedure (including video footage) and the Raman scattering can be found elsewhere.[40]

Steady state microwave discharges are generated in a tubular quartz reactor of 20 cm length and 3 cm inner tube diameter, inserted through the wide faces of a rectangular waveguide. This position corresponds to a maximum of the electric field in the center of the tube. The microwave generator supplies up to 1 kW continuous power at 2.45 GHz operating frequency. An E-H tuner is used for impedance matching of the waveguide with the plasma for maximizing the absorbed input power. Tangential gas injection stabilizes the plasma discharge in the center of the tube. This ensures operation over a wide parameter space while minimizing the heat load on the tube.

FTIR spectra were taken with a Varian 670 IR spectrometer at a resolution of  $0.5 \text{ cm}^{-1}$  and 32 average scans in a 20.9 cm long sampling cell equipped with KBr windows. To have a robust fitting of the acquired spectra the FTIR cell was placed at approximately 2 m downstream, allowing for the gas to cool down. A thermocouple was set at the same position as the FTIR cell, to confirm a constant temperature during the power scan.

The reactor conditions during the discharges were continuously logged (1Hz) with a data acquisition system. The pressure on-line acquisition system facilitated the measurements of molar flow changes from which hydrogen concentrations were independently obtained. Relating species distribution determined with FTIR and gas independent pressure measurements (strain gauge meter), we determined absolute concentration of all major species by sampling the entire reactor effluent stream.



(a)

**Figure 4:** Typical mass spectrometry sampling data shown as analog scan of the ionization current versus mass over charge ratio ( $m/z$ ). Plasma was generated at a pressure of 40 mbar, 5 slm  $\text{CH}_4$ , 0.5 slm Ar flow and 400 W input power. The peaks at  $m/z = 40, 20$  correspond to Ar.

On-going effluent mass spectrometry measurements were additionally taken, where Ar was fed at a level of 1% as an internal standard, as shown in Figure 4a. The complexity of the hydrocarbon cracking patterns inside the mass spectrometer made quantification difficult. Therefore, these measurements were only used for qualitative purpose.

## 2.2 Methodology

### 2.3 FTIR analysis of hydrocarbons yielding

The complex methane plasma chemistry is characterized by fitting individual hydrocarbon FTIR spectra to obtain absolute densities of the stable species. Figure 5 shows FTIR spectra recorded with plasma on and plasma off together and a diagram indicating the hydrocarbons present within the HITRAN database. Apart from  $\text{C}_2\text{H}_y$ ,  $\text{C}_3\text{H}_8$  and  $\text{C}_4\text{H}_2$  no other higher hydrocarbons are included within the HITRAN database.[41]  $\text{C}_3\text{H}_y$  or higher hydrocarbons are difficult to quantify with FTIR. Monitoring products with mass spectrometry learned that, the intensity corresponding to  $\text{C}_3$  and  $\text{C}_4$  groups was an order of magnitude lower than the one of  $\text{C}_2$  products, as shown in Figure 4. Similar low concentrations of  $\text{C}_x\text{H}_y (x > 2)$  were reported also in previous methane discharges in a microwave reactor.[26, 27]

Typical fitted spectra corresponding to the effluent detected hydrocarbons are shown in Figure 6. Regions of least interference from other species were selected for

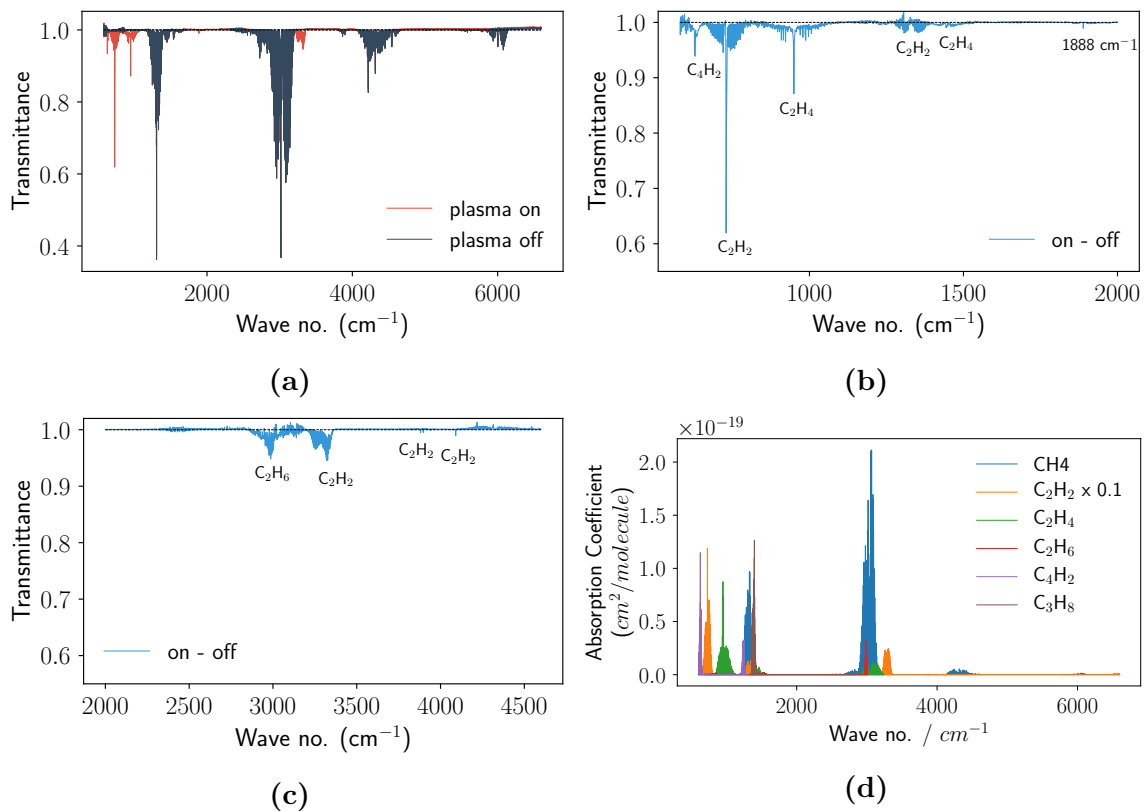


**Figure 5:** (a) Overview of plasma on (25 mbar, 300 W) and plasma off FTIR spectra. (b),(c) Zoom on the x-axis showing the reaction products ( $\text{C}_4\text{H}_2$ ,  $\text{C}_2\text{H}_2$ ,  $\text{C}_2\text{H}_4$  and  $\text{C}_2\text{H}_6$ ) by subtracting the plasma off from the plasma on spectra. (d) HITRAN overview of hydrocarbon absorption coefficients.[41]

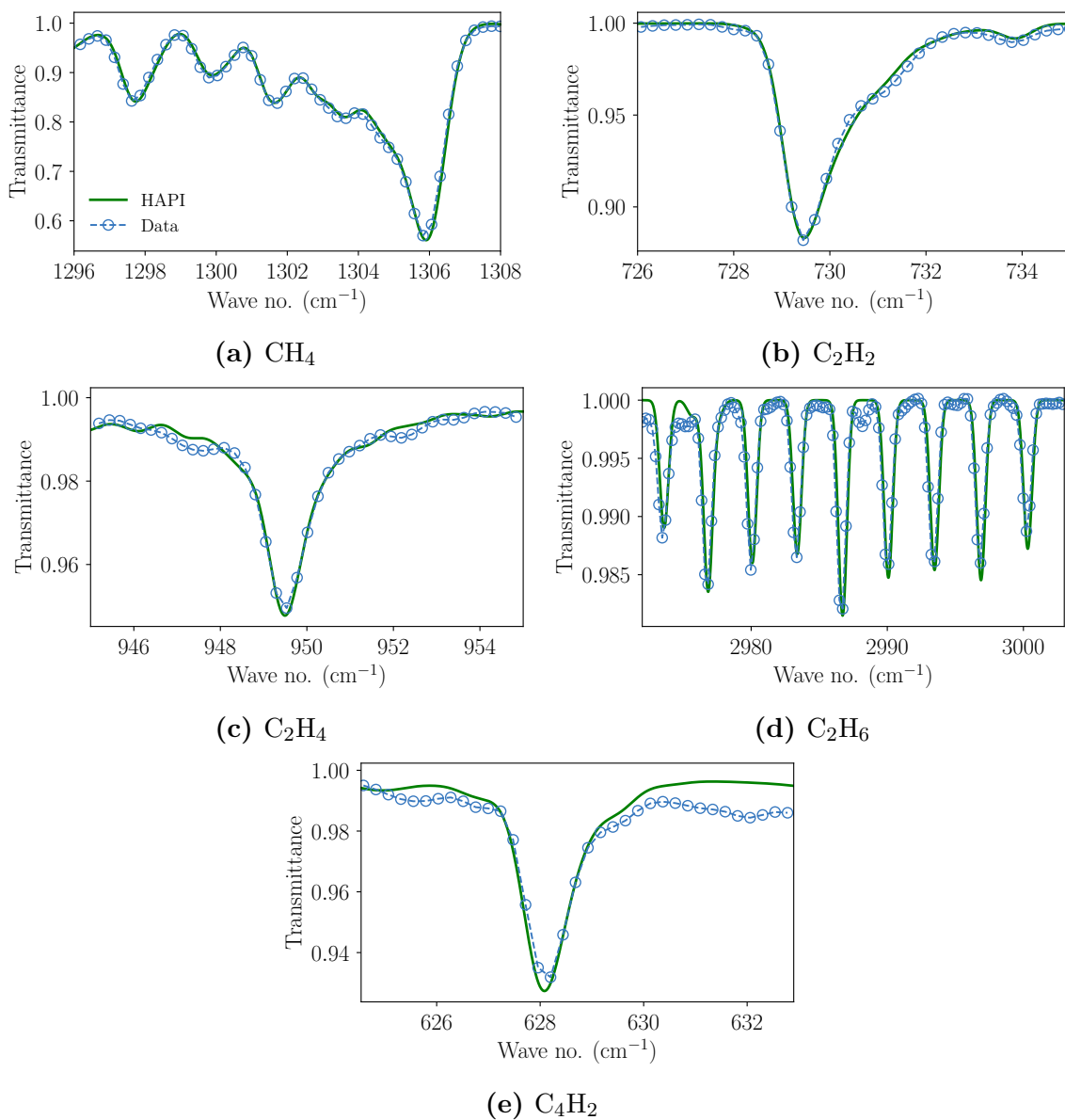


**Figure 6:** Sample FTIR fitted spectra for (a) methane, (b) acetylene, (c) ethylene, (d) ethane and (e) diacetylene. Resolution  $0.5\text{ cm}^{-1}$  and 32 scans. For the ethane window, the methane contribution was subtracted and the remaining spectrum offset to zero. The fitting is performed with the python routine HITRAN Application Programming Interface (HAPI).[41](The legend and color scheme are the same from (a)-(e)).

the fitting. For the ethane spectral region, the methane contribution was subtracted and the resulted transmittance background line was offset to unity. This region was selected in view of having the highest absorption cross section for ethane.

FTIR yields absolute densities of the resulted product distribution. Measurements of the effluent were taken sufficiently far downstream, where the gas has cooled down to room temperature, making the species density  $n_i$  the only free fit parameter. A least squares fit of the spectra was used to obtain species density according to the Beer-Lambert law for transmittance:

$$\tau_\nu = \exp(-n_i x \sigma_\nu) \quad (11)$$

where  $n_i x$  is the mass path (molecules/cm<sup>2</sup>) and  $\sigma_\nu$  is the absorption cross section (cm<sup>2</sup>/molecule) obtained from the HITRAN database. The HITRAN Application Programming Interface (HAPI) [41] python routine was used for fitting. Although all the main peaks could be well resolved, there were regions where adjacent lobes were present and could not be fitted, e.g. ethylene and diacetylene spectra in Figure 6c and 6e. However, this only contributed to the total error of the fit as the main peaks were the dominant ones. We have validated the FTIR results in our reactor discharges running on CH<sub>4</sub> in a comparison with a gas chromatography thermal conductivity detector/flame ionization detector (GC-TCD/FID). This proves the appropriateness of the approach.

## 2.4 Hydrogen concentration

Two approaches are used for inferring the hydrogen concentration present in the reactor, with their comparison yielding information on the reaction mechanism. The first one concerns particle balance calculations using pressure as a measurement for the molar flow change in the reactor. For a constant flow rate  $v_{\text{flow}}$  and gas temperature  $T$ , the pressure is a measure for the total molar flux inside the reactor

$$\Phi_{\text{CH}_4} = n_{\text{CH}_4} v_{\text{flow}} \quad (12)$$

where  $n_{\text{CH}_4}$  is the methane density. We verified that within the operating parameter space the flow rate was constant and that the gas has cooled down to room temperature.

In the absence of plasma the total pressure is:

$$\frac{p^{\text{off}}}{kT^{\text{off}}} = n_{\text{CH}_4}^{\text{off}} \quad (13)$$

where  $k$  is the Boltzmann constant and superscripts on and off refer to the plasma on and off phases. During plasma on phase, the total pressure becomes (by using the

ideal gas law):

$$\frac{p^{\text{on}}}{kT^{\text{on}}} = n_{\text{CH}_4}^{\text{on}} + \sum n_{\text{C}_x\text{H}_y} + n_{\text{H}_2} \quad (14)$$

where  $n_{\text{C}_x\text{H}_y}$  is hydrocarbon density and  $n_{\text{H}_2}$  is the hydrogen density.

For a constant gas temperature during plasma on and off phase at the measurements position, i.e. far downstream, the pressure difference ( $\Delta p = p_{\text{on}} - p_{\text{off}}$ ) reflects the increase in molar flow:

$$\frac{\Delta p}{kT} = \sum n_{\text{C}_x\text{H}_y} + n_{\text{H}_2} - (n_{\text{CH}_4}^{\text{off}} - n_{\text{CH}_4}^{\text{on}}). \quad (15)$$

As the pressure difference is recorded by the gas independent gauge meter and the hydrocarbon partial pressures follow from FTIR, we have established a relation for the hydrogen density:

$$n_{\text{H}_2} = \frac{\Delta p}{kT} - \sum n_{\text{C}_x\text{H}_y} + (n_{\text{CH}_4}^{\text{off}} - n_{\text{CH}_4}^{\text{on}}). \quad (16)$$

The second approach concerns closing the hydrogen balance based on stoichiometry of reaction set involved:

$$n_{\text{H}_2} = \frac{1}{2} \left( 4\beta n_{\text{CH}_4}^{\text{off}} - \sum y n_{\text{C}_x\text{H}_y} \right) \quad (17)$$

where  $\beta$  is the conversion degree.

In the same way, a carbon balance is made based on the FTIR detected product distribution (gas phase):

$$C_{\text{balance}} = \frac{n_{\text{CH}_4}^{\text{on}} + x \times n_{\text{C}_x\text{H}_y}}{n_{\text{CH}_4}^{\text{off}}} 100\%. \quad (18)$$

Ideally, if all the formed products are in the gas phase the carbon balance should add up to 100%. If not, we assume that the missing carbon is under the form of deposits (solid phase). We verify this assumption by comparison of the two hydrogen partial pressures, as given in equations 16-17.

## 2.5 Conversion, Selectivity and Energy Efficiency

The methane conversion (%) inside the microwave reactor follows from the depletion of gas flow via

$$\beta = \left( 1 - \frac{\Phi_{\text{CH}_4}^{\text{on}}}{\Phi_{\text{CH}_4}^{\text{off}}} \right) 100\% \quad (19)$$

where  $\Phi_{\text{CH}_4} = n_{\text{CH}_4} v_{\text{flow}}$  is the methane gas flow,  $n_{\text{CH}_4}$  is the methane density in the plasma on and off case and  $v_{\text{flow}}$  is the flow rate. For a constant flow rate (i.e. a linear dependence between pressure and flow) the conversion can be written as

$$\beta = \left( 1 - \frac{n_{\text{CH}_4}^{\text{on}}}{n_{\text{CH}_4}^{\text{off}}} \right) 100\% \quad (20)$$

where  $n_{\text{CH}_4}$  is the methane density in the plasma on and off case. In this way the conversion is expressed only in terms of the FTIR measured density. In a similar way, the selectivity towards product hydrocarbons (%) is defined as

$$S[\text{C}_x\text{H}_y] = x \frac{n_{\text{C}_x\text{H}_y}}{\beta n_{\text{CH}_4}^{\text{off}}} 100\% \quad (21)$$

where  $n_{\text{C}_x\text{H}_y}$  is the density of the formed hydrocarbons.

In most of the literature, the energy efficiency is given with respect to the acetylene formation, since reactors are commonly optimized for it.[24, 25, 26, 27] However, if there is a mix of selectivities it is necessary to account for all of the products in the energy efficiency calculations.[42, 43, 44] Hence, the energy efficiency is given by

$$\eta = \frac{\beta \Phi_{\text{CH}_4}^{\text{off}} \Delta H}{P_{\text{in}}} \quad (22)$$

where  $\Delta H$  is the total standard formation enthalpy and  $P_{\text{in}}$  is the input power

$$\Delta H = \sum \nu_{\text{mol}, \text{C}_x\text{H}_y} \Delta H_{\text{C}_x\text{H}_y}. \quad (23)$$

Finally, in view of comparison with other reactor types, it is useful to define also the specific energy input (SEI) as input power per methane flow

$$\text{SEI} = \frac{P_{\text{in}}}{\Phi_{\text{CH}_4}^{\text{off}}}. \quad (24)$$

## 2.6 Raman scattering

A detailed description of the setup, can be found elsewhere.[45] Basics of the process and usage as a gas temperature diagnostic in  $\text{N}_2\text{-CH}_4$  mixture discharges is given in the remainder of this section.

A frequency doubled ( $\lambda = 532 \text{ nm}$ ) Nd:YAG (Continuum Powerlite DLS 8000) laser operated at 4 W was used for Raman scattering. The beam was focused with an  $f = 2 \text{ m}$  lens along the axial direction of the reactor tube. Scattered light was collected at  $90^\circ$  with an achromatic doublet. A 1:1 image was projected onto a fibre bundle ( $27 \times 400 \mu\text{m}$ ) that is used to illuminate an custom built Littrow spectrometer

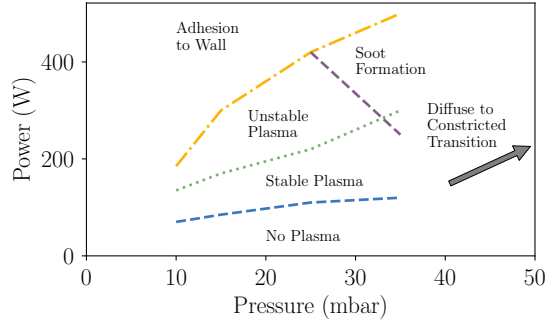


**Figure 7:** Schematic drawing of plasma boundaries in the diffuse operational regime: Soot formation, plasma expansion and adhesion to the wall (unstable), insufficient power to sustain plasma and diffuse to constricted transition.

( $f = 1$  m, lens diameter  $d = 100$  mm, dispersion of  $0.85$  nm mm $^{-1}$ ) equipped with an iCCD. A long pass filter with cut-off wavelength of  $550$  nm (ThorLabs FGL550) was placed in front of the collection fibres to block scattered light at the laser wavelength.

Raman scattering is an inelastic process in which the scattered light has different energy than that of the incident radiation due to interaction with molecules whose polarizability is modified by the electric field of the incident radiation. Upon interaction with the scatterers, the incident light can either gain or lose a discrete amount of energy proportional to the change in the vibrational ( $\nu$ ) and/or rotational ( $J$ ) quantum number induced in the non-resonant Raman transition. For the nitrogen molecule it is straightforward to calculate synthetic spectra and fit each detected peak, resulting in a gas temperature measurement.[45] On the other hand, for the methane molecule, it is a rather difficult task due to overlapping transitions given the higher number of vibrational modes and low resolution of the spectrometer.[46] We used the  $N_2$  molecule as probing molecule for the rotational temperature in  $N_2-CH_4$  mixture discharges.

### 3 Results

Visual observations showed that there are several operational boundaries in the microwave methane plasma, as shown in Figure 7. Data was acquired in scans of power, from  $50$  to  $550$  W, at three pressures of approximately  $15$ ,  $25$  and  $35$  mbar, and two gas flows  $4$  and  $8$  slm. These settings were selected for being favorable for having low gas temperatures and deposit yields. The lowest power (used with the lowest pressure and flow settings) corresponded to the minimum input needed to sustain the plasma. The power upper limit was given by the volumetric expansion of the plasma

switching to a discharge mode touching the wall (unstable plasma). The low pressure conditions kept the plasma discharge mode in the diffuse regime.[47] The motivation to stay within the diffuse regime is a practical one. Within the constricted regime, deposit layers form on the quartz tube which limit operational time to only minutes. Visually, the tube appears to be deposited from the downstream side of the discharge. Within a few minutes, depending on the intensity of the discharge conditions, this layer crawls upstream into the waveguide region, leading to the microwave radiation being mainly absorbed by the deposited layer.

The pressure increase in the microwave plasma leads to a transition between a diffuse and constricted regime. It is difficult to find the exact pressure boundary where this transition happens because the plasma goes off when the pressure is gradually increased, at constant input power. The constricted regime could be observed by increasing the pressure in a stepwise manner up to 100 mbar, at an input power of 500 W and 6 slm flow. Plasma color changed from purple to bright yellow, similar to a flame, with soot formation completely covering the reactor in a matter of minutes. For comparison, in CO<sub>2</sub> discharges this transition was observed at about 130 mbar. The conditions were assessed in CO<sub>2</sub> microwave discharge by monitoring the spontaneous emission from the plasma with a CCD camera.[47, 36]

The nature of these regimes comes from theory of microwave propagation for different electron neutral collision frequency  $\nu_{e-n}$ . In the diffuse regime the electron density is fixed by the cut off frequency of the propagating wave 2.45 GHz at  $n_e = 7.5 \times 10^{16} \text{ m}^{-3}$  with the plasma volume increasing to satisfy the power balance. In the constricted regime, an arc like discharge, the plasma volume appears more or less fixed and the electron density increases linearly with input power.

### 3.1 Carbon and Hydrogen Balances

Based on the product distribution, the following set of reactions was used for calculating the hydrogen and carbon balance due to the methane conversion process:



The hydrogen balance yields the hydrogen concentration that was further compared with the values obtained from the pressure based measurements, as shown in Figure 8a. Figure 8b shows in a consistency plot, that a good agreement is obtained

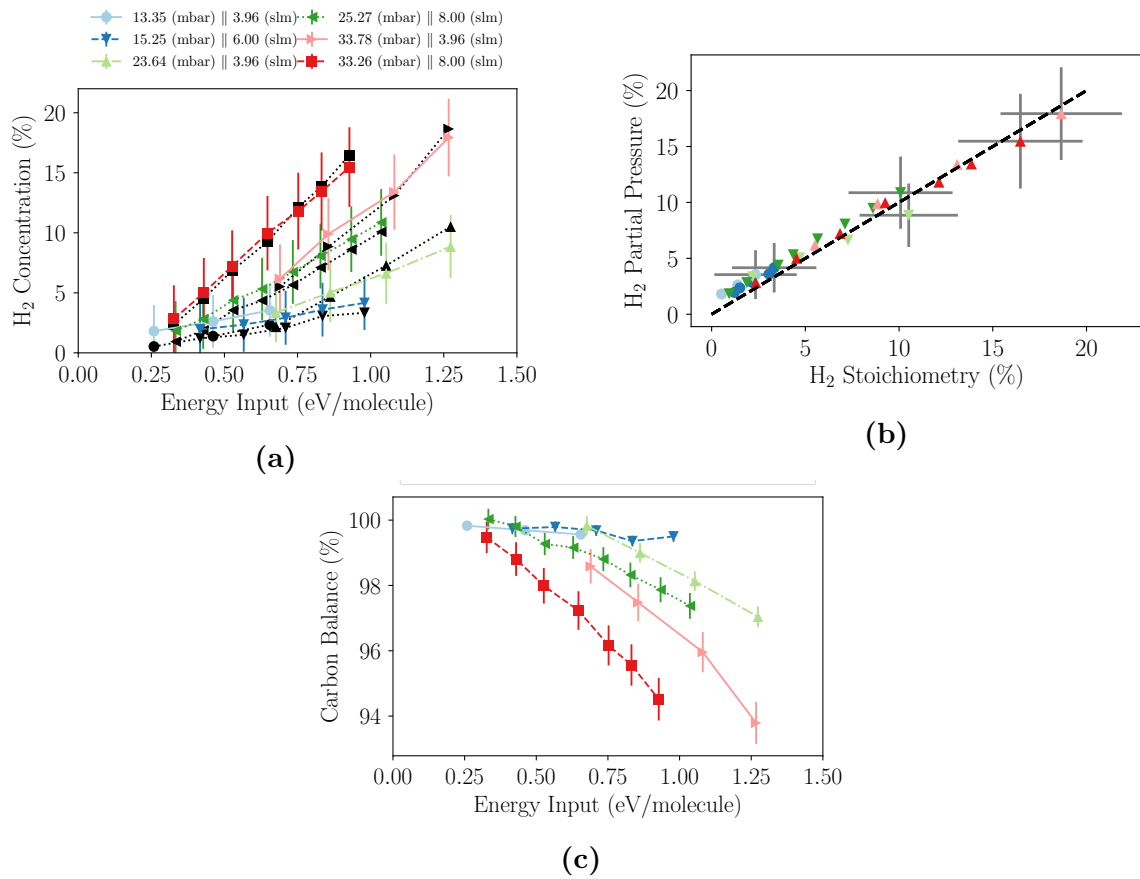


**Figure 8:** Hydrogen and carbon balance based on reactions 25 - 29. (a) Hydrogen balance obtained from the stoichiometry of the reaction set represented in color. Hydrogen balance obtained from the absolute pressure measurement represented in black. (b) Consistency plot for hydrogen concentrations. The black dashed  $y=x$  line is given as reference (c) Carbon balance (the legend and color coding is the same for (a) to (c) graphs).

for these two approaches. The y-axis represents the concentration from the pressure gauge measurements (first approach) and the x-axis the concentration derived from carbon balance based on the stoichiometry (second approach). The agreement confirms that the deposits formation can be attributed to reaction 29.

The carbon balance is done for FTIR detected products (gas phase), reactions 25-28, as shown in Figure 8c. The missing component, i.e. a carbon balance below 100%, yields the undetected solid phase carbon according to reaction 29. In view of the low expected concentrations for undetected  $C_xH_y$  ( $x > 2$ ) it is likely that the missing carbon to be mainly due to deposits. From this measured carbon balance, deposition rates up to 0.6 mg/s are estimated. For an average discharge of 10 minutes, approximately 0.36 g of deposits should have been accumulated inside all over the reactor.

Weighing measurements underestimate the amount of deposits formed. The deposition process was performed by a  $CH_4$  plasma discharge at a power of 1kW, gas flow at 12 slm (SEI of 1.16 eV/molecule), and pressure of 60 mbar to maximize the amount of deposits. After 2 minutes of deposition, the tube turned black completely. The amount of carbon deposited was found to be 0.014 g by weighing the tube before and after deposition. FTIR deposits are estimated at 0.072 g for the same amount of time, at a lower pressure of 35 mbar and similar SEI. It is likely that deposits reached further downstream of the tube, on other components of the vacuum system.

### 3.2 Conversion and Energy Efficiency

Conversion and energy efficiency increase with both input power and pressure. Figure 9 shows an overview of reactor performance, based on the equations defined in subsection 2.5. Conversion increases linearly with SEI, having approximately equal slopes per data pressure set, as shown in the inset of the Figure 9a, except for a last (stray)point at 34.41 mbar and 3.96 slm. The offset in the x-axis is interpreted as minimum power needed to sustain plasma. Additional to dissociation the input power is also lost into other channels such as ionization, heat or radiation. For the higher pressures this intercept is around 125 W, while for the lower pressure it corresponds to 70 W.

There are two driving forces of the conversion process: plasma and thermal chemistry. These can be intertwined so that is difficult to say which one is dominant. Thermal chemistry is determined by the gas temperature. Almost a linear temperature increase with both pressure and power were reported based on optical emission spectroscopy (OES) from the  $C_2$  Swan and  $H_2$  Fulcher- $\alpha$  band for pulsed microwave methane plasma experiments.[27, 28] Details on methane thermochemistry and gas temperature measurements are presented in the following sections.

The effect of plasma conditions on conversion could come from the increase of the

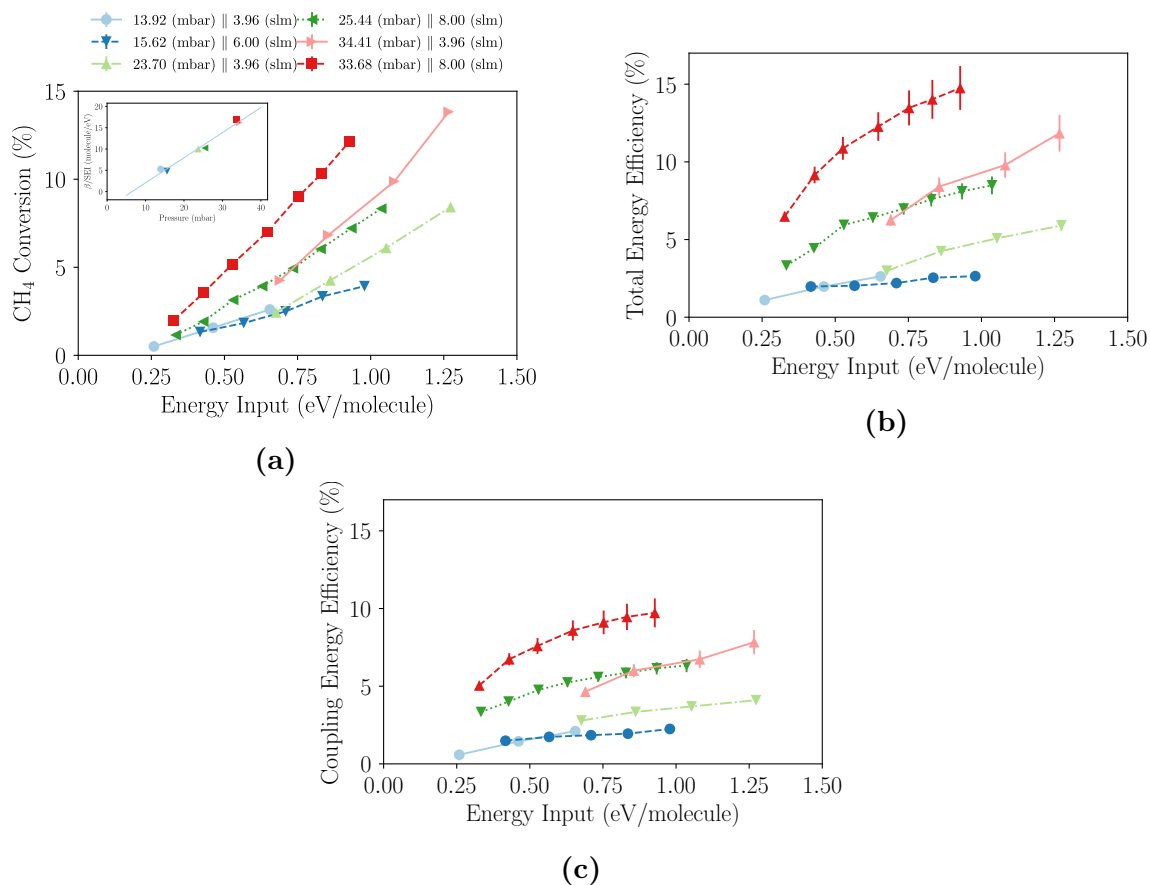


**Figure 9:** Overview of reactor performance based on FTIR data obtained for a scan of power, pressure, and flow. (a) Methane conversion determined from depletion; inset shows slope of conversion lines versus pressure. (b) Total energy efficiency, including deposits formation. (c) Coupling energy efficiency, excluding deposits formation. The legend and color scheme are the same from (a) and (c).

plasma density or volume with power, where a larger part of the gas flow is treated. In the diffuse regime the plasma density is more or less set at the microwave cut off frequency value. In addition, the plasma is radially expanding with power. Hence, it is likely that the volume increase with power to be part of the conversion driving force. Similar behavior has been reported in CO<sub>2</sub> microwave discharges as well.[47] This behavior can be better understood by looking at the power balance inside the plasma:[48]

$$P_{\text{in}} = n_0 n_e V \sum k_i U_i \quad (30)$$

where,  $n_0$  and  $n_e$  are the neutral and electron density,  $V$  is the plasma volume and the summation represents the main electron loss channels. Text book plasma physics says that the electron temperature does not depend on the input power, being set by particle balance.[48] Hence, the plasma volume increases to accommodate the input power while maintaining a constant densities product  $n_0 n_e$ .

The rate of conversion with SEI increases also linearly with pressure as shown in the inset of the Figure 9a. This rate multiplied with the total enthalpy, represents the energy efficiency of the entire conversion process, as shown by the Equation 22 and plotted as total efficiency in Figure 9b. The coupling efficiency is calculated by taking into account only the product hydrocarbons (i.e. excluding deposits), as shown in Figure 9c. The two efficiencies increase with input power and pressure, with highest values corresponding to conditions where acetylene selectivity is highest. The standard enthalpy of formation for acetylene is highest among the formed products, resulting in an efficiency increase with acetylene selectivity .

Doubling the flow results in differences only for the higher pressure. At the same specific energy input, a shorter residence time results in a higher conversion (and energy efficiency). Normally, shorter residence time must lead to lower conversion degrees. The higher power density corresponding to the same SEI overcompensates the shorter residence time resulting in a higher conversion. This behavior is attributed to an increased contribution of the thermal conversion. Higher power densities lead to increased gas temperatures where thermal effects are enhanced.

### 3.3 Selectivity of Hydrocarbons

Figure 10 shows the hydrocarbons selectivities. The carbon based selectivities are calculated among the gas phase products only (i.e. equivalent to normalized quantities). Prior to normalization, the deposits selectivity can be calculated, as shown in Figure 10d. For all discharge conditions the sum of the absolute selectivities was lower than 100 % and the remainder was considered as deposits selectivities. We decided to show gas phase selectivities only, i.e. 100% minus the deposits selectivities.

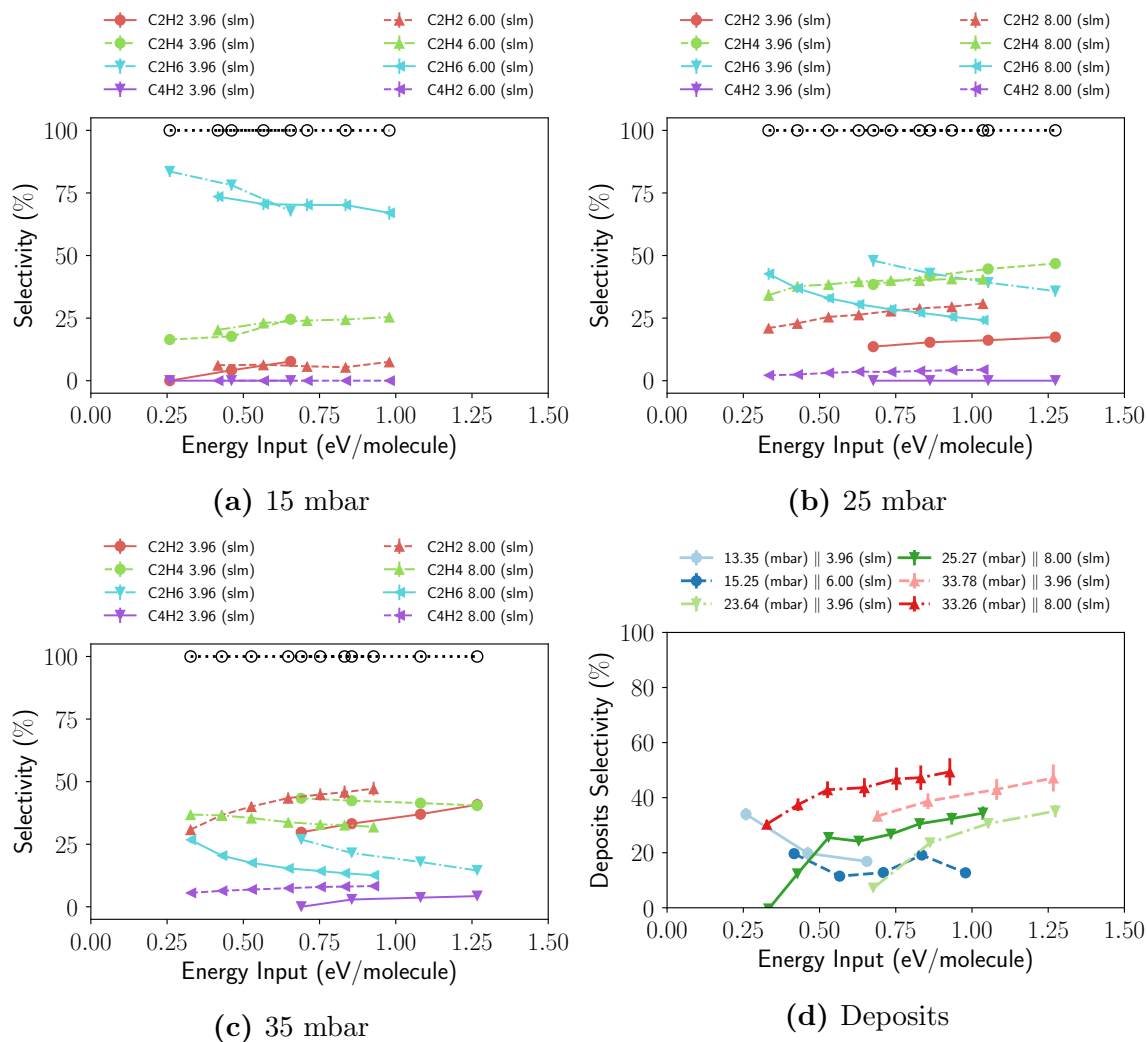


**Figure 10:** Selectivities grouped by pressure for acetylene, ethylene, ethane and diacetylene at: (a) 15 mbar, (b) 25 mbar and (c) 35 mbar. Selectivities are obtained from measuring absorption signatures of each individual hydrocarbon. Figure (d) shows the deposits selectivity for all three pressure ranges, based on carbon balance calculations

Thus we normalized the resulted values such that the sum of measured selectivities is always 100 %, as shown by the black dashed lines in Figure 10a-10c.

Hydrocarbon selectivities are grouped by pressure with ethane showing the highest value, up to 80 % (60 % when deposits are included) at the lowest pressure. Ethane has a very small molar fraction on the order of  $10^{-3}$  in the equilibrium picture of methane conversion, as shown in Figure 12. Although methane chemistry is rather complex with multiple pathways leading to product formation, the high ethane selectivity can only be attributed to methyl radical formation and subsequent recombination.[49, 50, 51, 52, 27]

Selectivity shifts towards acetylene with both power and pressure. With increasing power ethane selectivity decreases while ethylene and acetylene selectivities show the opposite. The effect is even more pronounced at higher pressures. Increasing pressure results in the same selectivity shift to less saturated hydrocarbons and deposits. Dehydrogenation of the more saturated hydrocarbons, ethane and ethylene, towards acetylene and deposits is likely to be the responsible mechanism. Both conversion and gas temperature increase with pressure and power. Increased conversion leads to formation of more atomic hydrogen radicals available to react with the formed products as well. Additionally, dehydrogenation reaction rates have an approximately square dependence with gas temperature.[38]

An alternative pathway involves a change in the radical distribution, as shown by the equations 1-4. Methylene and methylidyne radicals ( $\text{CH}_2$  and  $\text{CH}$ ) can further recombine to form ethylene and acetylene. The change in radical distribution could be due to an increase in electron temperature or more likely due to dehydrogenation as well. With increased conversion, dehydrogenation could apply to methyl radicals leading to a shift in product selectivity.

Diacetylene formation adds further insight into the methane chemistry at play. It was also previously observed in small quantities in glow discharges of methane using radical and ion scavengers at pressures up to 10 Torr.[53] A potential formation path involves the reaction of ethynyl radicals and acetylene:



The increase in acetylene selectivity is responsible for both the formation of ethynyl radical and coupling to diacetylene. At the same time, acetylene and diacetylene are known as soot precursors where the initial formation steps are accompanied by the presence of polycyclic aromatic hydrocarbons (PAHs).[54, 55] We note the correlation between the formation of diacetylene and deposits in the reactor. An additional important factor in growth of the aromatics and soot formation is presented by the gas temperature.

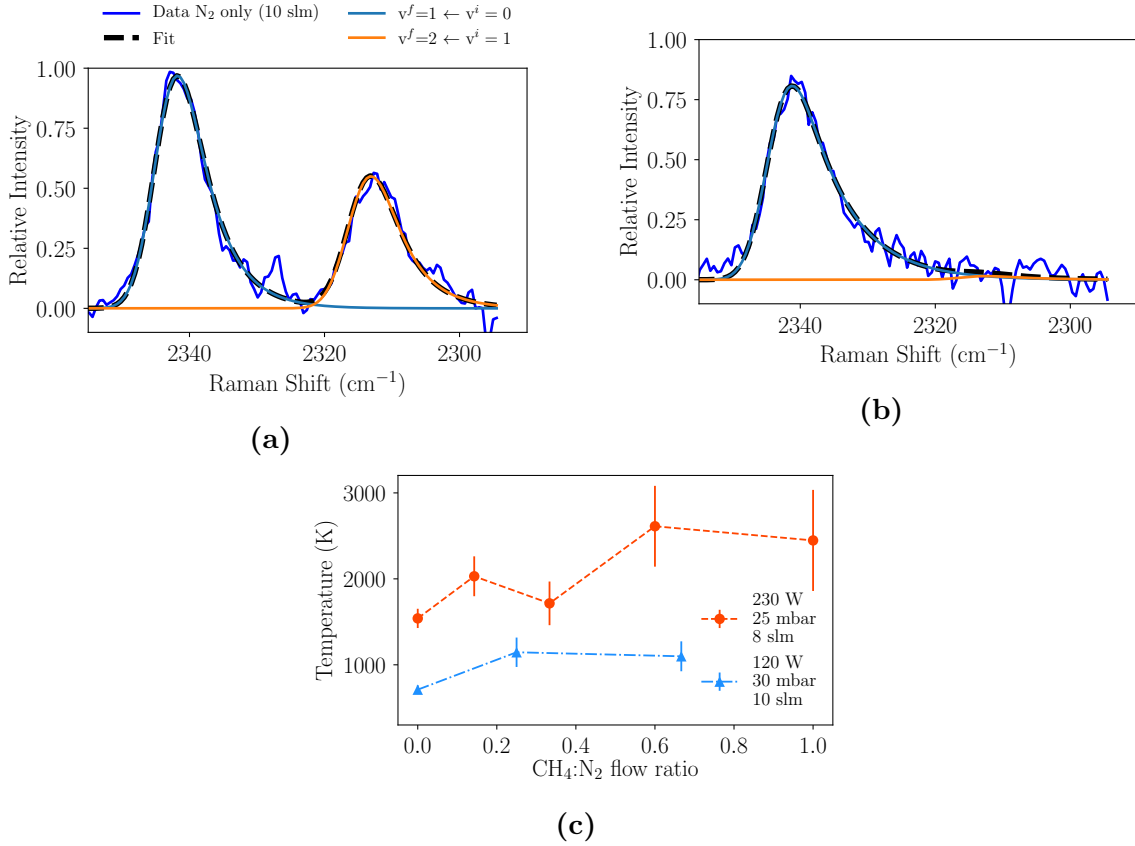


**Figure 11:** Ro-vibrational Raman spectra measured in the effluent of (a) pure N<sub>2</sub> and (b) N<sub>2</sub>:CH<sub>4</sub>=1:1 plasma (in the axial center of the tube, at +10 mm downstream the end of the waveguide; 30 mbar and 120 W input power). (c) Rotational temperature measurements from Raman scattering in N<sub>2</sub> - CH<sub>4</sub> plasma mixtures. Fitting was done with the same python routine as described elsewhere.[45]

### 3.4 Gas Temperature measurements

In literature optical emission spectroscopy (OES) studies from the C<sub>2</sub> Swan and H<sub>2</sub> Fulcher- $\alpha$  band, a linear temperature increase from 1500 K to 2500 K with SEI from 2 eV/molecule to 8 eV/molecule at 30 mbar were reported for pulsed microwave methane plasma experiments.[27, 28] Rotational temperature is determined from Boltzmann plots versus energy levels in the ground and excited states of C<sub>2</sub> and H<sub>2</sub>. Although this method is more suitable at higher pressures (for fast equilibration times of the excited states with ground state molecules) a good agreement was found between the two “thermometer” molecules.

Gas temperatures are measured in-situ by vibrational Raman scattering on N<sub>2</sub> in

mixtures of N<sub>2</sub>-CH<sub>4</sub>. Compared to e.g. C<sub>2</sub> Swan and H<sub>2</sub> Fulcher- $\alpha$  spectroscopy, a widely used method to retrieve the same information, this has the advantage that it does not depend on the assumptions regarding the rotational equilibrium of excited C<sub>2</sub>/H<sub>2</sub> species with the gas mixture. In addition, it is not line integrated and has thus superior spatial resolution.

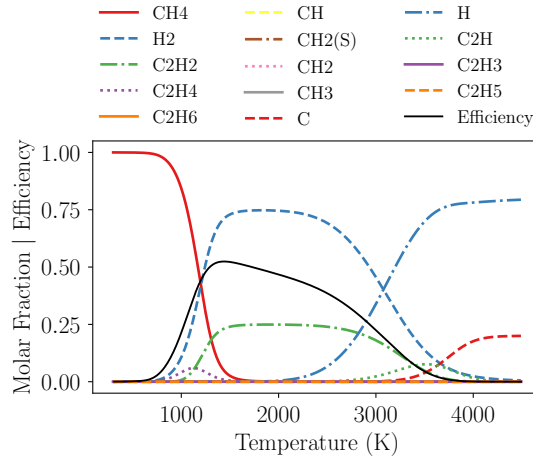
Figure 11 shows an overview of the vibrational Raman measurements in N<sub>2</sub> and N<sub>2</sub>-CH<sub>4</sub> mixtures. Figure 11a shows the vibrational Raman spectrum measured in pure N<sub>2</sub> discharges. Keeping the same discharge conditions but adding methane into the reactor yields the spectrum shown in Figure 11b. Adding methane to the discharge increases the overall gas temperature. The increase could be due to the fact that the vibrational VT relaxation rate coefficient  $k_{VT}^{10}(T_0=300\text{ K})$  for methane is a factor of  $3 \times 10^4$  higher than in nitrogen. [25]

Figure 11c shows gas temperature measurements as function of the methane to nitrogen gas flow ratio. The 120 W discharge was at 30 mbar and 10 slm total flow (0.17 eV/molecule) and the 230 W discharge was at 25 mbar and 8 slm total flow (0.4 eV/molecule). In both cases, adding CH<sub>4</sub> to pure N<sub>2</sub> discharges resulted in elevated gas temperatures. Increasing the methane content up to 50 % of the mixture led to a slight increase in temperature. In view of the sensitivity of the Raman scattering diagnostic, decreasing further the N<sub>2</sub> content towards a pure CH<sub>4</sub> discharge was not possible. Given that methane set the gas temperature we assumed that the N<sub>2</sub>:CH<sub>4</sub> mixture to be representative for plasma with pure methane as well. A more substantial temperature increase is seen with input power from approximately 1000 K up to 2500 K. The gas temperatures are obtained in the center of the plasma and, therefore, represent maximum temperatures. In our previous work, on pure N<sub>2</sub> microwave plasma assessed by spatially resolved Raman scattering measurements, cooling rates on the order of 30 Kcm<sup>-1</sup> have been measured.[45]

Additionally, we have measured the FTIR product distribution of plasma discharges for equimolar N<sub>2</sub>-CH<sub>4</sub> mixtures. Overall the C<sub>2</sub> chemistry for the N<sub>2</sub>:CH<sub>4</sub>=1:1 mixture discharge at 28 mbar was similar to the pure methane discharge results. For the same energy input interval, the conversion degree was highest for the mixture case. However, the energy efficiency was not. More than double in the conversion degree of the mixture is necessary to beat the pure methane discharge efficiency. Selectivities remained similar to the 25 mbar pressure cases.

### 3.5 Methane thermochemistry

In this section we determine the thermal equilibrium composition of methane as benchmark for the plasma driven chemistry. At different temperatures and medium pressure the efficiency corresponding to the C<sub>x</sub>H<sub>y</sub> production is calculated as well. Thermal equilibrium of methane discharges in the context of plasma conversion refers



**Figure 12:** Simplified methane thermodynamic equilibrium composition (carbon solid phase not included) and the instantaneous quenching efficiency for hydrocarbon production as function of temperature at a pressure of 100 mbar. The simulations are based on GRI-Mech 3.0 mechanism and were performed with Cantera.[38, 56]

only to the heavy particles (i.e. molecules, ions and radicals). The electron energies are estimated to be an order of magnitude higher than the equivalent gas temperatures.[48]

Cantera is a specialized computer programme for chemical kinetics, thermodynamics, and transport processes. It is used here to calculate the equilibrium composition based on the GRIMech 3.0 mechanism.[56, 38] Figure 12 shows methane thermodynamic equilibrium composition together with the instantaneous quenching efficiency (i.e. assumes that the equilibrium composition can be preserved) for the produced hydrocarbons as function of temperature at a pressure of 100 mbar. The energy efficiency was defined in the methodology part in Equation 22 subsection 2.2.

The dissociation of methane starts at temperatures higher than 700 K and is complete at 1500 K. There is a window where ethylene appears as a minor product, but the main formed products are acetylene and hydrogen. Subsequently, further decomposition occurs into atomic hydrogen and carbon. The endothermic process of methane conversion into acetylene has a maximum of 52.43 % thermal efficiency at 1440 K. After that, the production of acetylene is rather constant with most of the input energy going into heat of the gas mixture. The theoretical values assume ideal quenching and also a homogeneous reactor temperature. This simplified methane thermodynamic equilibrium excludes the solid phase carbon formation



When this is included, the equilibrium phase is made only of solid carbon and molec-

ular hydrogen.[57, 23]

The peaked temperature profile causes that full dissociation is only reached in the hot core of the microwave reactor and that the global conversion remains limited. This effect together with the gas flow dynamics has been described for  $\text{CO}_2$  in detail by den Harder et al..[47] Regarding selectivity, most likely there is an interplay between plasma and thermal chemistry where plasma generates radicals and final distribution is set by thermodynamics. Mild discharges where ethane has high selectivities are more prone to be due to the plasma methyl radical formation followed by self recombination. At higher power discharges and higher gas temperature, thermal effects become stronger making the final distribution to resemble more the equilibrium calculations.

## 4 Conclusions

A consistent data set of methane reduction in a continuous microwave plasma reactor was obtained for which a complete analysis was made on stable product distribution and reactor performance. FTIR was used to measure absolute concentrations of the major hydrocarbon species. In addition, hydrogen concentration was also independently inferred from pressure based change in molar flow measurements. From the stoichiometry of the reactions, the amount of deposits was obtained as well as by closing both the carbon and hydrogen balance.

A mild discharge regime characterized by low energy input and pressure aimed at having conditions favorable for nonequilibrium plasma chemistry. In spite of that, high gas temperatures up to 2500 K were measured from vibrational Raman scattering on  $\text{N}_2$  probing molecules in  $\text{N}_2 - \text{CH}_4$  mixture discharges. Energy efficiency reached up to 15 %, of which 10 % represented coupling efficiency, with remaining of the energy going into heat.

Hydrocarbon selectivities were grouped by pressure. At the lowest pressure ethane had the highest selectivity up 60 % (80 % based on gas phase species only). Selectivity shifted towards lower saturated hydrocarbons and deposits formation with both power and pressure. At the same time conversion increased. The initial formation of products was plasma dominated through the nature of the created radicals. Increasing thermal effects are likely to be responsible for the selectivity shift. Hydrogen abstraction reactions have a square dependence on temperature leading to a change in both radical, from  $\text{CH}_3$  to  $\text{CH}_2$  and  $\text{CH}$ , and product distribution.

## References

- [1] Anders Holmen. Direct conversion of methane to fuels and chemicals. *Catalysis Today*, 142(1-2):2–8, 2009.
- [2] ISIC. Ethylene uses and market data, 2017. URL <https://www.icis.com/resources/news/2007/11/05/9075777/ethylene-uses-and-market-data/>.
- [3] TECHNIP. Ethylene production, 2017. URL <http://www.technip.com>.
- [4] Jan van de Loosdrecht, F.G. Botes, Ionel Mugurel Ciobîcă, Alta Ferreira, P Gibson, Denzil Moodley, Abdool Saib, Jacobus Visagie, C Weststrate, and Hans Niemantsverdriet. Fischer–tropsch synthesis: Catalysts and chemistry, 08 2013.
- [5] FG Botes, JW Niemantsverdriet, and J Van De Loosdrecht. A comparison of cobalt and iron based slurry phase Fischer–Tropsch synthesis. *Catalysis today*, 215:112–120, 2013.
- [6] I Chokendoff and JW Nimantsverdrief. Concepts of modern catalysis and kinetics 2nd, revised and enlarged edition, 2007.
- [7] Pei Tang, Qingjun Zhu, Zhaoxuan Wu, and Ding Ma. Methane activation: the past and future. *Energy & Environmental Science*, 7(8):2580–2591, 2014.
- [8] Helmut Schwarz. Activation of methane. *Angewandte Chemie International Edition*, 30(7):820–821, 1991.
- [9] Derek HR Barton. The invention of chemical reactions. *ChemInform*, 21(40), 1990.
- [10] Robert H Crabtree. Aspects of methane chemistry. *Chemical reviews*, 95(4): 987–1007, 1995.
- [11] Raimund Horn and Robert Schlögl. Methane activation by heterogeneous catalysis. *Catalysis Letters*, 145(1):23–39, 2015.
- [12] G. E. Keller and M. M. Bhasin. Synthesis of ethylene via oxidative coupling of methane. i. determination of active catalysts. *Journal of Catalysis*, 73(1):9–19, 1982. ISSN 10902694. doi: 10.1016/0021-9517(82)90075-6.
- [13] J. H. Lunsford. The catalytic conversion of methane to higher hydrocarbons. *Catalysis Today*, 1990. ISSN 09205861. doi: 10.1016/0920-5861(90)85004-8.

- [14] S.J. Korf, J.a. Roos, L.J. Veltman, J.G. van Ommen, and J.R.H. Ross. Effect of additives on lithium doped magnesium oxide catalysts used in the oxidative coupling of methane. *Applied Catalysis*, 56(1):119–135, 1989. ISSN 01669834. doi: 10.1016/S0166-9834(00)80163-3. URL <http://linkinghub.elsevier.com/retrieve/pii/S0166983400801633>.
- [15] John A Sofranko, John J Leonard, and C Andrew Jones. The oxidative conversion of methane to higher hydrocarbons. *Journal of catalysis*, 103(2):302–310, 1987.
- [16] Sergei Pak, Ping Qiu, and Jack H Lunsford. Elementary reactions in the oxidative coupling of methane over Mn/Na<sub>2</sub>WO<sub>4</sub>/SiO<sub>2</sub> and Mn/Na<sub>2</sub>WO<sub>4</sub>/MgO catalysts. *Journal of Catalysis*, 179(1):222–230, 1998.
- [17] Takahito Nishiyama and Ken-Ichi Aika. Mechanism of the oxidative coupling of methane using CO<sub>2</sub> as an oxidant over PbO-MgO. *Journal of Catalysis*, 122(2):346 – 351, 1990. ISSN 0021-9517. doi: [https://doi.org/10.1016/0021-9517\(90\)90288-U](https://doi.org/10.1016/0021-9517(90)90288-U). URL <http://www.sciencedirect.com/science/article/pii/002195179090288U>.
- [18] Saeed Al-Zahrani, Qi Song, and Lance L Lobban. Effects of carbon dioxide during oxidative coupling of methane over lithium/magnesia: mechanisms and models. *Industrial & engineering chemistry research*, 33(2):251–258, 1994.
- [19] Kevin J Smith and Jan Galuszka. Effect of carbon dioxide on methane oxidative coupling kinetics. *Industrial & engineering chemistry research*, 33(1):14–20, 1994.
- [20] Jack H Lunsford. Catalytic conversion of methane to more useful chemicals and fuels:a challenge for the 21st century. *Catalysis Today*, 63:165–174, 2000. ISSN 09205861. doi: 10.1016/S0920-5861(00)00456-9.
- [21] Yide Xu, Xinhe Bao, and Liwu Lin. Direct conversion of methane under nonoxidative conditions. *Journal of Catalysis*, 216(1-2):386–395, 2003. ISSN 00219517. doi: 10.1016/S0021-9517(02)00124-0.
- [22] Heinz Gladisch. How Huels makes acetylene by DC arc. *Hydrocarbon Process. Petrol. Refiner*, 41:159–164, 1962.
- [23] J. R. Fincke, R. P. Anderson, T. Hyde, B. A. Detering, R. Wright, R. L. Bewley, D. C. Haggard, and W. D. Swank. Plasma thermal conversion of methane to acetylene. *Plasma Chemistry and Plasma Processing*, 22(1):107–138, 2002. ISSN 02724324. doi: 10.1023/A:1012944615974. URL <http://www.springerlink.com/content/n281038422m01740/%5Cnhttp://link.springer.com/10.1023/A:1012944615974>.

- [24] A.A. Fridman, A.I. Babaritskiy, V.K. Givotov, S.A. Dyomkin, S.A. Nester, and V.D. Rusanov. Babaritsky. page 6, Bochum, 1991. ISPC-10.
- [25] Alexander Fridman. *Plasma Chemistry*. 2008. doi: 10.1017/CBO9780511546075. URL <http://books.google.com/books?hl=en&lr=&id=ZzmtGEHCC9MC&oi=fnd&pg=PR39&dq=Plasma+chemistry&ots=YhbAAcm08f&sig=iHC2mizqtafrUBFdPIMf50p6bvA>.
- [26] M Heintze and M Magureanu. Efficient methane conversion to acetylene. *HAKONE 8: International Symposium on High Pressure, Low Temperature Plasma Chemistry*, 1 and 2:201–205, 2002. URL [https://inis.iaea.org/search/search.aspx?orig\\_q=RN:33065207](https://inis.iaea.org/search/search.aspx?orig_q=RN:33065207).
- [27] M Heintze, M Magureanu, and M Kettlitz. Mechanism of C<sub>2</sub> hydrocarbon formation from methane in a pulsed microwave plasma. *Journal of applied physics*, 92(12):7022–7031, 2002.
- [28] Vasile I Pârvolescu, Monica Magureanu, and Petr Lukes. *Plasma chemistry and catalysis in gases and liquids*. John Wiley & Sons, 2012.
- [29] Steven L. Suib and Richard P. Zerger. A direct, continuous, low-power catalytic conversion of methane to higher hydrocarbons via microwave plasmas, 1993. ISSN 00219517. URL <http://www.sciencedirect.com/science/article/pii/S0021951783710341>.
- [30] Jurgen Meichsner, Martin Schmidt, Ralf Schneider, and Hans-Erich Wagner. *Nonthermal plasma chemistry and physics*. CRC Press, 2012.
- [31] Hayashi database, 2017. URL [www.lxcat.net](http://www.lxcat.net).
- [32] Shigeru Kado, Kohei Urasaki, Yasushi Sekine, Kaoru Fujimoto, Tomohiro Nozaki, and Ken Okazaki. Reaction mechanism of methane activation using non-equilibrium pulsed discharge at room temperature. *Fuel*, 82(18):2291 – 2297, 2003. ISSN 0016-2361. doi: [https://doi.org/10.1016/S0016-2361\(03\)00163-7](https://doi.org/10.1016/S0016-2361(03)00163-7). URL <http://www.sciencedirect.com/science/article/pii/S0016236103001637>.
- [33] Tomohiro Nozaki, Akinori Hattori, and Ken Okazaki. Partial oxidation of methane using a microscale non-equilibrium plasma reactor. *Catalysis Today*, 98(4):607 – 616, 2004. ISSN 0920-5861. doi: <https://doi.org/10.1016/j.cattod.2004.09.053>. URL <http://www.sciencedirect.com/science/article/pii/S0920586104006133>.

- [34] Tomohiro Nozaki, Nahoko Muto, Shigeru Kado, and Ken Okazaki. Dissociation of vibrationally excited methane on Ni catalyst: Part 1. Application to methane steam reforming. *Catalysis Today*, 89(1):57–65, 2004.
- [35] A. I. Florescu-Mitchell and J. B A Mitchell. Dissociative recombination. *Physics Reports*, 430(5-6):277–374, 2006. ISSN 03701573. doi: 10.1016/j.physrep.2006.04.002.
- [36] G. J. van Rooij, D. C. M. van den Bekerom, N. den Harder, T. Minea, G. Berden, W. A. Bongers, R. Engeln, M. F. Graswinckel, E. Zoethout, and M. C. M. van de Sanden. Taming microwave plasma to beat thermodynamics in CO<sub>2</sub> dissociation. *Faraday Discuss.*, 183:233–248, 2015. doi: 10.1039/C5FD00045A. URL <http://dx.doi.org/10.1039/C5FD00045A>.
- [37] Louis S Kassel. The thermal decomposition of methane1. *Journal of the American Chemical Society*, 54(10):3949–3961, 1932.
- [38] Gri-mech. <http://combustion.berkeley.edu/gri-mech/>. Accessed: 2017-10-02.
- [39] RK Janev and D Reiter. Collision processes of CH<sub>y</sub> and CH<sub>y</sub><sup>+</sup> hydrocarbons with plasma electrons and protons. *Physics of Plasmas*, 9(9):4071–4081, 2002.
- [40] Dirk van den Bekerom, Niek den Harder, Teofil Minea, Nicola Gatti, Jose Palomares Linares, Waldo Bongers, Richard van de Sanden, and Gerard van Rooij. Non-equilibrium microwave plasma for efficient high temperature chemistry. *Journal of Visualized Experiments*, (126):1–11, 2017. ISSN 1940-087X. doi: 10.3791/55066. URL <https://www.jove.com/video/55066/non-equilibrium-microwave-plasma-for-efficient-high-temperature>.
- [41] R. V. Kochanov, I. E. Gordon, L. S. Rothman, P. Wcisło, C. Hill, and J. S. Wilzewski. Hitran application programming interface (hapi): A comprehensive approach to working with spectroscopic data. *Journal of Quantitative Spectroscopy and Radiative Transfer*, 177:15–30, 2016. ISSN 00224073. doi: 10.1016/j.jqsrt.2016.03.005.
- [42] Aimin Zhu, Xiuling Zhang, Weimin Gong, and Bao’an Zhang. Study on Coupling of Methane under Pulse Corona Plasma in the Presence of Oxygen. *Acta Physico - Chimica Sinica*, 16(9):842–843, 2000. ISSN 10006818. doi: 10.1007/BF03027312.

- [43] A Oumghar, JC Legrand, AM Diamy, N Turillon, and RI Ben-Aim. A kinetic study of methane conversion by a dinitrogen microwave plasma. *Plasma Chemistry and Plasma Processing*, 14(3):229–249, 1994.
- [44] Gui-Bing Zhao, Sanil John, Ji-Jun Zhang, Linna Wang, Suresh Muknahallipatna, Jerry C Hamann, John F Ackerman, Morris D Argyle, and Ovid A Plumb. Methane conversion in pulsed corona discharge reactors. *Chemical Engineering Journal*, 125(2):67–79, 2006.
- [45] Nicola Gatti, Srinath Ponduri, Floran Peeters, Dirk Cornelis Maria van den Bekerom, Teofil Minea, Paolo Tosi, Richard Van de Sanden, and Gerard J Van Rooij. Preferential vibrational excitation in microwave nitrogen plasma assessed by raman scattering. *Plasma Sources Science and Technology*, 2018. URL <http://iopscience.iop.org/10.1088/1361-6595/aabd60>.
- [46] Eric Jourdanneau, Frederic Chaussard, Robert Saint-Loup, Tony Gabard, and Hubert Berger. The methane raman spectrum from 1200 to 5500 cm<sup>-1</sup>: A first step toward temperature diagnostic using methane as a probe molecule in combustion systems. *Journal of Molecular Spectroscopy*, 233(2):219–230, 2005.
- [47] Niek den Harder, Dirk van den Bekerom, Richard S Al, Martijn F Graswinckel, Jose M Palomares, Floran JJ Peeters, Srinath Ponduri, Teofil Minea, Waldo A Bongers, Mauritius van de Sanden, et al. Homogeneous CO<sub>2</sub> conversion by microwave plasma: Wave propagation and diagnostics. *Plasma Processes and Polymers*, 14(6), 2017.
- [48] Michael A Lieberman and Alan J Lichtenberg. *Principles of plasma discharges and materials processing*. John Wiley & Sons, 2005.
- [49] Wen L Hsu. Gas-phase kinetics during microwave plasma-assisted diamond deposition: Is the hydrocarbon product distribution dictated by neutral-neutral interactions? *Journal of applied physics*, 72(7):3102–3109, 1992.
- [50] CG Schwärzler, O Schnabl, J Laimer, and H Störi. On the plasma chemistry of the C/H system relevant to diamond deposition processes. *Plasma Chemistry and Plasma Processing*, 16(2):173–185, 1996.
- [51] Kh Hassouni, O Leroy, S Farhat, and A Gicquel. Modeling of H<sub>2</sub> and H<sub>2</sub>/CH<sub>4</sub> moderate-pressure microwave plasma used for diamond deposition. *Plasma Chemistry and Plasma Processing*, 18(3):325–362, 1998.

- [52] L Mechold, J Röpcke, X Duten, and A Rousseau. On the hydrocarbon chemistry in a H<sub>2</sub> surface wave discharge containing methane. *Plasma Sources Science and Technology*, 10(1):52, 2001.
- [53] K Hiraoka, K Aoyama, and K Morise. A study of reaction mechanisms of methane in a radio-frequency glow discharge plasma using radical and ion scavengers. *Canadian journal of chemistry*, 63(11):2899–2905, 1985.
- [54] Kin M Leung, Rune P Lindstedt, and WP Jones. A simplified reaction mechanism for soot formation in nonpremixed flames. *Combustion and flame*, 87(3-4): 289–305, 1991.
- [55] Michael Frenklach. Reaction mechanism of soot formation in flames. *Physical chemistry chemical Physics*, 4(11):2028–2037, 2002.
- [56] David G. Goodwin, Harry K. Moffat, and Raymond L. Speth. Cantera: An object-oriented software toolkit for chemical kinetics, thermodynamics, and transport processes. <http://www.cantera.org>, 2017. Version 2.3.0.
- [57] James R Fincke, Raymond P Anderson, Timothy A Hyde, and Brent A Detering. Plasma pyrolysis of methane to hydrogen and carbon black. *Industrial & Engineering Chemistry Research*, 41(6):1425–1435, 2002.